

Characterization of a GAGG detector for neutron measurements in underground laboratories

L. Ascenzo^{1,3}, G. Benato^{2,3}, Y. Chu^{2,3}, G. Di Carlo³, A. Molinario^{4,5},
S. Vernetto^{4,5}

¹Università degli Studi dell'Aquila, Via Vetoio 42, L'Aquila, 67100, Italy.

²Gran Sasso Science Institute, Viale F. Crispi 7, L'Aquila, 67100, Italy.

³INFN - Laboratori Nazionali del Gran Sasso, Via G. Acitelli 22 Assergi (AQ), 67100, Italy.

⁴INAF - Osservatorio Astrofisico di Torino, Via Osservatorio 20, Pino Torinese (TO),
10025, Italy.

⁵INFN - Sezione di Torino, Via P. Giuria 1, Torino, 10125, Italy.

Contributing authors: lorenzo.ascenzo@student.univaq.it; giovanni.benato@gssi.it;
yingjie.chu@gssi.it; giuseppe.dicarlo@lngs.infn.it; andrea.molinario@inaf.it;
vernetto@to.infn.it;

Abstract

In rare events experiments, such as those devoted to the direct search of dark matter, a precise knowledge of the environmental gamma and neutron backgrounds is crucial for reaching the design experiment sensitivity. The neutron component is often poorly known due to the lack of a scalable detector technology for the precise measurement of low-flux neutron spectra. $\text{Gd}_3\text{Al}_2\text{Ga}_3\text{O}_{12}$ (GAGG) is a newly developed, high-density scintillating crystal with a high gadolinium content, which could allow to exploit the high (n, γ) cross section of ^{155}Gd and ^{157}Gd for neutron measurements in underground environments. GAGG crystals feature a high scintillation light yield, good timing performance, and the capability of particle identification via pulse-shape discrimination. In a low-background environment, the distinctive signature produced by neutron capture on gadolinium, namely a β/γ cascade releasing up to 9 MeV of total energy, and the efficient particle identification provided by GAGG could yield a background-free neutron capture signal. In this work, we present the characterization of a first GAGG detector prototype in terms of particle discrimination performance, intrinsic radioactive contamination, and neutron response.

Keywords: Neutron detection, GAGG detector, underground experiments

1 Introduction

In the field of rare events searches, a precise knowledge of the environmental backgrounds is fundamental for the design of appropriate shieldings for the experiments. Among the possible background sources, neutrons are often poorly known due to

the lack of an affordable detector technology for the measurement of low-flux neutron spectra from thermal energies to 10 MeV.

The last decade has witnessed the development of several garnet scintillation crystals containing gadolinium, which has the two isotopes – ^{155}Gd and ^{157}Gd – with the highest neutron capture

cross section. These crystals are now available with dimensions suitable for the use as particle detectors. GAGG is of particular interest for its high scintillation light yield, good timing performance, high density (6.6 g/cm^3) and capability of particle identification via pulse-shape discrimination [1–4]. In a low cosmic-ray environment, e.g. an underground laboratory, the distinctive signature produced by neutron capture on gadolinium, namely a γ -ray cascade releasing $\sim 9 \text{ MeV}$ of total energy, and the efficient particle identification provided by GAGG would yield a background-free neutron signal.

Thanks to its 50.9% gadolinium mass fraction, the application of GAGG as a neutron detector is being considered by the scientific community [5–9]. However, all tests performed so far have involved small-size GAGG crystals, with a volume of up to a few cm^3 , hence the considered neutron signature consisted of X-rays and low-energy γ -rays from Gd de-excitation. Exploiting the recent availability of crystals of $\sim 100 \text{ cm}^3$ volume, and the most up-to-date developments on Monte Carlo simulations of gamma ray cascades produced by neutron capture reactions [10–12], we aim at demonstrating the possibility of detecting directly in the GAGG crystal the high-energy γ -rays following the neutron capture on ^{155}Gd and ^{157}Gd . In this perspective, the neutron signature is a β/γ event in the range between 2.6 MeV, corresponding to the endpoint of natural γ radioactivity, and $\sim 9 \text{ MeV}$, corresponding to the endpoint of the γ cascades from the Gd isotopes. When operated in Bonner spheres, such a detector would allow to perform neutron spectroscopy in low-background environments, and could represent a valid alternative to the well-established ^3He proportional counters, whose price and availability on the market have fluctuated significantly over the last decades.

In this article, we present the characterization of a first detector prototype, consisting of a $\sim 100 \text{ cm}^3$ GAGG crystal, read-out with a photomultiplier (PMT), operated underground in the Hall A of the Gran Sasso National Laboratory (LNGS) of INFN, Italy, between January and October, 2024. In Sec. 2 we describe the experimental setup and the measurements performed. In Sec. 3 we detail the data processing and detector performance. In Sec. 4 and 5 we report on the background characterization and on the

source and environmental neutron measurements. Finally, in Sec. 6 we provide a plan for the future developments of the detector.

2 Detector and data taking

The detector prototype is composed of a cylindrical GAGG:Ce crystal with 5 cm diameter and 5 cm height, corresponding to a mass of 0.65 kg, coupled to a Hamamatsu R2257 PMT and mounted in a custom-made stainless steel case (Fig. 1). To maximize the light collection, the crystal is wrapped in Vikuiti ESR reflector foil. The PMT is supplied with -1.4 kV using a CAEN V6533N high-voltage module, and $2 \mu\text{s}$ long signal waveforms are read-out at 250 MHz using a 14-bit CAEN V1725 digitizer. The GAGG scintillation signal features a fast decay constant of $\sim 90 \text{ ns}$, and a slow one of $\sim 400 \text{ ns}$, with the ratio of the fast and slow component depending on the interacting particle (see later, Fig. 4).

For the purpose of measuring γ events above 2.6 MeV, it is crucial to operate the detector underground to bypass the otherwise overwhelming background from cosmic muons, and to discriminate them from α events which could represent a background in our region of interest. Our choice of sampling time and window length is thus motivated by the need to distinguish α from β/γ particles via pulse-shape discrimination.

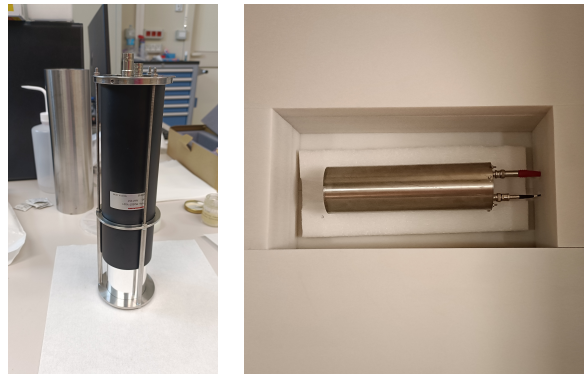


Fig. 1: Left: the detector during assembly, with the PMT on the top and the GAGG crystal wrapped in reflector foil in the bottom. Right: the detector enclosed in its stainless steel case and installed in the borated PE shielding.

We performed several measurements aimed at a full characterization of the detector response and background, and at a first evaluation of its performance as a neutron detector. We started with γ calibrations using ^{232}Th , ^{238}U and ^{241}Am sources, then placed the detector in a 20 cm thick polyethylene (PE) shielding with 5% boron loading, depicted in Fig. 1, and acquired background data for ~ 2.5 months. We then performed two calibration runs with an AmBe neutron source inside the shielding: in the first run we placed a 5 cm thick PE moderator between the source and the detector; in a second run we removed the PE moderator, and placed a 5 cm thick Cu layer between the source and the detector to shield the 4.4 MeV γ -ray produced by the AmBe source itself. In addition, we acquired data for one month with the completely unshielded detector to measure the thermal neutron flux in Hall A of LNGS. Finally, we acquired again background data for ~ 1 month using a 400 ns acquisition window for a more precise evaluation of the ^{232}Th contamination in the crystal, as detailed in Sec. 4. A summary of the performed measurements is given in Tab. 1.

Table 1: List of measurements performed with the GAGG prototype detector.

Measurement description	Duration
^{232}Th calibration	
^{238}U calibration	
^{241}Am calibration	
Background (with 20 cm borated PE)	77.5 days
AmBe with 5 cm PE	21.5 hr
AmBe with 5 cm Cu γ shield	22.5 hr
Environmental (thermal) neutrons	31.6 days
Background with 400 ns window	27 days

3 Data processing

We process the data using the Octopus software [13], originally developed for the reconstruction of data from bolometric detectors and further expanded for analyzing the signals from the GAGG detector. We evaluate the energy of each triggered event by integrating the waveform, and reject events with a trigger shifted from its predefined 0.45 μs position in the waveform as well as events with an unstable baseline. The combination of these two cuts remove $\sim 1\%$ of the events.

We show in Fig. 2 the calibration spectra collected with ^{238}U , ^{232}Th and ^{241}Am sources placed in front of the detector. We fit the most prominent peaks in the calibration spectra, and extracted the resolution curve reported in Fig. 3, indicating an asymptotic relative full width at half maximum (FWHM) of $\sim 4.2\%$ in the region of interest for the Gd de-excitation γ rays, i.e. above 3 MeV.

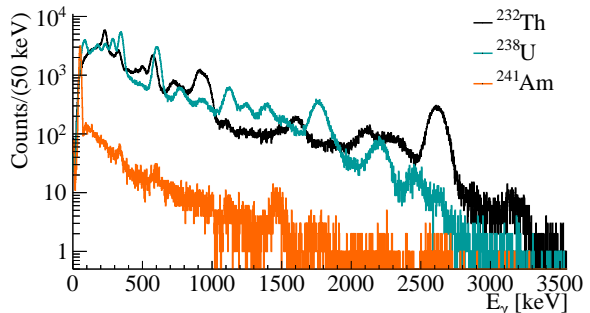


Fig. 2: Calibration spectra recorded with ^{232}Th (black), ^{238}U (teal) and ^{241}Am (orange) sources placed in front of the detector. The only visible signature produced by ^{241}Am is the 59.5 keV peak reconstructed in the very left of the spectrum. The orange continuum is induced by the internal and environmental β/γ background.

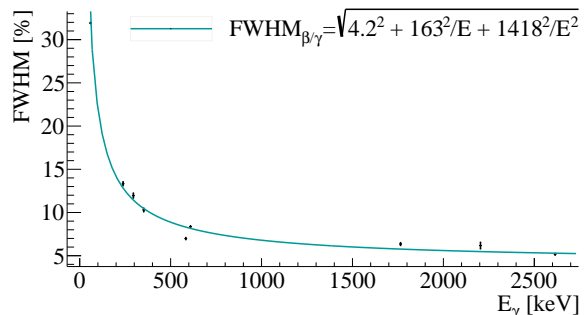


Fig. 3: Resolution curve obtained from the most prominent peaks visible in the ^{232}Th , ^{238}U , and ^{241}Am spectra.

The discrimination between β/γ and α events is based on the different pulse shape of the two event types, which is evident from Fig. 4 (top). Rather than exploiting the commonly used mean-decay-time algorithm [14], which is sensitive to the trigger position within the digitized window,

we opted to develop a pulse-shape discrimination (PSD) algorithm using the events power spectrum, as shown in the bottom of Fig. 4, thus completely bypassing any possible misalignment of the events within the acquisition window. Specifically, we compute the χ^2 between the power spectrum of each single event w_f and the average power spectrum \bar{w}_f of γ events:

$$\chi^2 = \sum_{f=0}^{f_{max}} (w_f - A_{\chi^2} \cdot \bar{w}_f)^2 \quad , \quad (1)$$

where f indicates the frequency index of the discrete power spectrum, and A_{χ^2} is a normalization factor against which χ^2 is minimized. Such a normalization factor will be proportional to the pulse integral I (computed in the time domain) for β/γ events, and significantly deviate from it for α events.

The distribution of the PSD variable A_{χ^2}/I as a function of energy is divided in two separate bands for the β/γ and α events, as shown in Fig. 5 for background data. This figure also shows that the energy of α events is quenched at the $\sim 15\%$ level with respect to β/γ events, a value similar to what reported in literature [15].

4 Background characterization

We apply the PSD cut to the 77.5 days of background data, obtaining the β/γ and α spectra depicted in Figs. 6 and 7, respectively. The β/γ spectrum features two prominent γ lines, corresponding to the 1460 keV peak from ^{40}K and to the 2615 keV peak from ^{208}Tl . The continuum between them is attributable to external γ 's from the ^{232}Th and ^{238}U decay chains undergoing Compton scattering in the crystal, and β and γ 's emitted and fully absorbed within the crystal itself.

A second, less intense continuum reaching 5 MeV is visible: we ascribe it to a ^{232}Th contamination in the crystal, which eventually leads to the presence and decay of ^{208}Tl . In fact, the signature from a ^{208}Tl decaying outside the crystal would be a combination of mono-energetic γ lines at 2615 keV and 583 keV, plus their sum and Compton continua. On the other hand, the signature from a ^{208}Tl nucleus decaying inside the

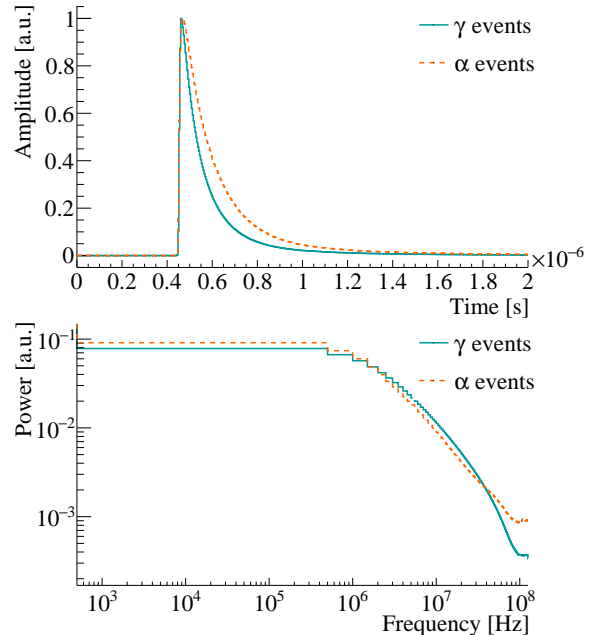


Fig. 4: Normalized average pulse (top) and average power spectrum (bottom) for β/γ and α events.

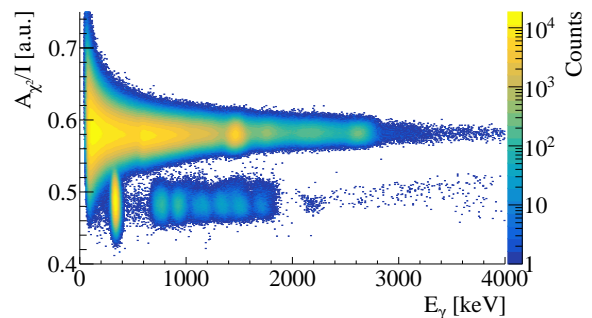


Fig. 5: Distribution of the PSD variable A_{χ^2}/I as a function of energy for background data. The upper horizontal band corresponds to β/γ events, the lower one to α events.

crystal is a β with energy up to 1.8 MeV plus possibly the full absorption of the 583 and 2615 keV γ . The latter are emitted in coincidence in 85% of the cases and have an overall probability of $\sim 50\%$ to be fully contained in the GAGG crystal under study. As a consequence, we expect a continuum reaching the Q -value of the ^{208}Tl decay, 5 MeV. To our knowledge, no other isotope – either long-lived or belonging to a decay chain – could induce such a β/γ background.

Finally, 22 events with $E_\gamma > 5$ MeV are detected. The expected number of events induced by muons crossing the crystal, which would cover a much wider energy range reaching ~ 70 MeV, is $\lesssim 5$. Moreover, we expect environmental neutrons to be fully absorbed by the borated PE shield. Hence, we estimate that 80% of the events above 5 MeV are induced by neutrons produced e.g. by (α, n) reactions in the detector setup and subsequently captured by ^{155}Gd or ^{157}Gd . Overall, the background in the $[5, 10]$ MeV region is (0.28 ± 0.06) events/day.

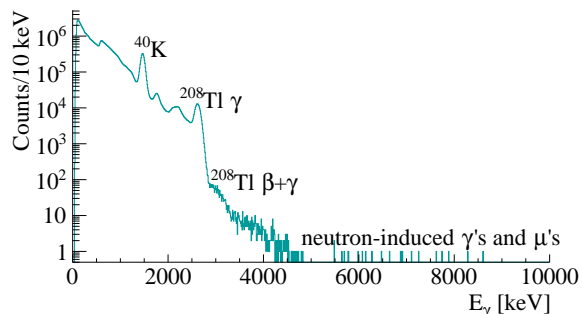


Fig. 6: Background spectrum in the β/γ band. The continuum between the ^{208}Tl line and 5 MeV can be ascribed to the pile-up of β and γ decays from ^{208}Tl . Events at energies above 5 MeV are due to γ 's emitted following neutron captures on Gd, and residual muons.

The α spectrum (Fig. 7) features three main components. A prominent peak is visible at roughly 240 keV of the γ energy scale (E_γ), with a rate of 1 event/s. About half of these events can be attributed to ^{152}Gd , decaying α with a Q -value of 2205 keV. The other half are thought to be induced by a crystal contamination of ^{147}Sm , that decays α with a Q -value of 2311 keV. ^{147}Sm was indeed found to be a contaminant in two Gd samples measured via Inductively Coupled Plasma Mass Spectrometry (ICP-MS) [16].

A set of six bumps, some of which are clearly composed of overlapping components, is present at $E_\gamma \in [700, 1900]$ keV. After a careful analysis of the α spectrum, which is detailed below, we conclude that the leftmost two peaks are induced by the early parts of the ^{232}Th and ^{238}U decay chains, and the other four correspond to various α 's emitted by the late part of the ^{232}Th chain, the early

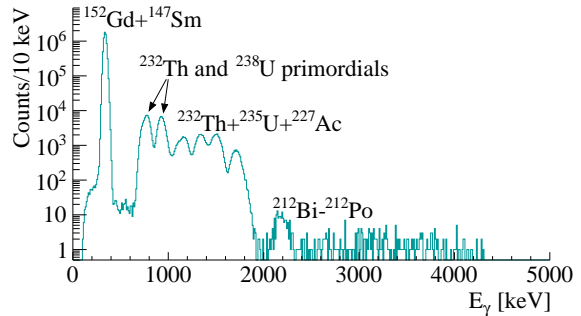


Fig. 7: Background spectra in the α band, here represented in the γ energy scale E_γ . The first peak is originated from the ^{152}Gd and ^{147}Sm α decays. The six bumps in the central part comes from various α decays from the ^{232}Th , ^{238}U , and ^{235}U chains. The small peak at $E_\gamma = 2.2$ MeV and the sparse continuum up to 4.5 MeV are due to the pile-up of ^{212}Bi β/γ and ^{212}Po α decays.

part of ^{235}U chain, and by a ^{227}Ac contamination of the crystal.

A small peak is present at $E_\gamma \simeq 2200$ keV, followed by a sparse continuum reaching 4400 keV. This component is due to the pile-up of ^{212}Bi and ^{212}Po decay events from the ^{232}Th chain, which are reconstructed within the same $2 \mu\text{s}$ acquisition windows and are composed of an α and a β/γ event. This interpretation is supported by the fact that the PSD distribution of these events (Fig. 5) gets broader with energy and slowly drifts towards the β/γ band.

The interpretation and energy calibration of the α spectrum is particularly complicated by the energy dependence of the α quenching. To identify the individual α components, we search for time-delayed coincidences (TDC) between subsequent α events [17, 18] belonging to the ^{238}U , ^{235}U and ^{232}Th decay chains, reported in Tab. 2. This analysis is sensitive to TDCs with half-life values ranging from the length of the signal window ($2 \mu\text{s}$) to a few times the inverse of the event rate in the α band, which is about 30 s. For much longer half-life values, the occurrence of random delayed coincidences would become dominant.

For a first identification of the α peaks, we search for the fastest α - α TDC, corresponding to $^{219}\text{Rn} \rightarrow ^{215}\text{Po} \rightarrow ^{211}\text{Pb}$. We compute the time delay Δt between subsequent α events in a suitable range of pulse integrals I , and plot it against the pulse integral of the first event in the pair,

Table 2: List of TDC belonging to the ^{238}U , ^{235}U and ^{232}Th decay chains, with half-life values less than 5 min.

Progenitor	Decay	Q-value [keV]	Half-life [s]
^{235}U	$^{223}\text{Ra} \rightarrow ^{219}\text{Rn} + \alpha$	5979	$1.78 \cdot 10^{-3}$
	$^{219}\text{Rn} \rightarrow ^{215}\text{Po} + \alpha$	6946	
	$^{215}\text{Po} \rightarrow ^{211}\text{Pb} + \alpha$	7526	
^{232}Th	$^{224}\text{Ra} \rightarrow ^{220}\text{Rn} + \alpha$	5789	55.6 0.1442
	$^{220}\text{Rn} \rightarrow ^{216}\text{Po} + \alpha$	6405	
	$^{216}\text{Po} \rightarrow ^{212}\text{Pb} + \alpha$	6906	
^{232}Th	$^{212}\text{Bi} \rightarrow ^{212}\text{Po} + \beta$	2252	$2.99 \cdot 10^{-7}$
	$^{212}\text{Po} \rightarrow ^{208}\text{Pb} + \alpha$	8954	
^{232}Th	$^{212}\text{Bi} \rightarrow ^{208}\text{Tl} + \alpha$	6207	183
	$^{208}\text{Tl} \rightarrow ^{208}\text{Pb} + \beta$	4999	
^{238}U	$^{222}\text{Rn} \rightarrow ^{218}\text{Po} + \alpha$	5590	186
	$^{218}\text{Po} \rightarrow ^{214}\text{Pb} + \alpha$	6115	
^{238}U	$^{214}\text{Bi} \rightarrow ^{214}\text{Po} + \beta$	3269	$1.64 \cdot 10^{-4}$
	$^{214}\text{Po} \rightarrow ^{210}\text{Pb} + \alpha$	7834	

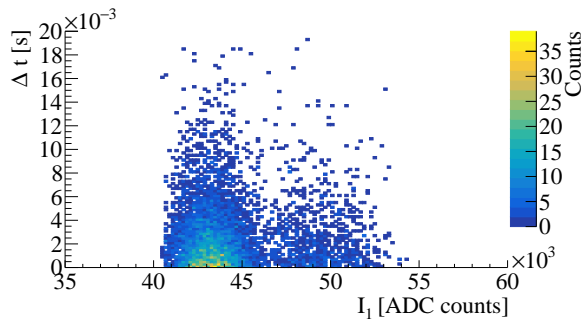


Fig. 8: Distribution of Δt between the ^{219}Rn and ^{215}Po α decays vs. the pulse integral I_1 of ^{219}Rn . A clear exponential decay in time is evident in $I_1 \in [4, 4.7] \cdot 10^4$, indicating the presence of ^{219}Rn . The other population at $I_1 \in [4.7, 5.3] \cdot 10^4$ is due to ^{219}Rn decays in which both α and γ are emitted (11% of the cases).

I_1 . If the ^{219}Rn triplet is present, we expect a large number of events in a well-defined range of pulse integral for $\Delta t < 10$ ms (corresponding to about 5 times the half-life of ^{215}Po). The background from random delayed coincidences should be negligible in this time window. Moreover, the ^{215}Po would produce an exponentially decreasing distribution of Δt , while random coincidences would only produce a flat distribution. Figure 8 shows the presence of two populations centered

Table 3: Half-life values reconstructed from the identified TDCs, compared with the expected values obtained from literature [19].

Isotope	Measured $T_{1/2}$	Expected $T_{1/2}$
^{219}Rn	3.83 ± 0.08 s	3.96 s
^{215}Po	1.77 ± 0.03 ms	1.78 ms
^{220}Rn	55 ± 1 s	56 s
^{216}Po	141 ± 2 ms	144 ms

around $I_1 = 4.3 \cdot 10^4$ and $I_1 = 4.9 \cdot 10^4$, with an exponentially decaying Δt . Both correspond to the $^{219}\text{Rn} \rightarrow ^{215}\text{Po}$ TDC, with the first population composed of pure α events, and the second of α events accompanied by a low-energy γ de-excitation which significantly shifts I_1 to larger values thanks to the higher light-yield of β/γ events. We then reconstruct the Δt distribution between α events including events both backward and forward in time to have an accurate estimation of the background level. We finally fit the resulting distribution with an exponential plus a flat background B :

$$f(\Delta t) = A \exp\left(-\frac{\ln 2 \cdot \Delta t}{T_{1/2}}\right) + B \quad ,$$

where $T_{1/2}$ is the half-life of the second isotope of the doublet. The same procedure is repeated to look for the other α decay of the triplet. The fits to the time delay distributions for $^{223}\text{Ra} \rightarrow ^{219}\text{Rn}$ and $^{219}\text{Rn} \rightarrow ^{215}\text{Po}$ α decays are shown in Fig. 9.

We apply this method also to the second α triplet, from the ^{232}Th chain. The measured half-life values of the decays are consistent with the expected ones for both α triplets, as reported in Tab. 3. This is a robust confirmation of the correct identification of the α decays.

We also search for the α - α TDC from $^{222}\text{Rn} \rightarrow ^{218}\text{Po} \rightarrow ^{214}\text{Pb}$ and the β - α TDC from $^{214}\text{Bi} \rightarrow ^{214}\text{Po} \rightarrow ^{210}\text{Pb}$, both belonging to the ^{238}U chain, finding no candidate event. This indicates that the lower part of the ^{238}U chain is not present in the GAGG crystal under study. Similarly, we search for the $^{212}\text{Bi} \rightarrow ^{208}\text{Tl} \rightarrow ^{208}\text{Pb}$ doublet from the ^{232}Th chain, but find no excess of signal events over a very high background induced by the β candidate events.

At this point, we use the identified α peaks to calibrate the α energy scale. Specifically, we fit

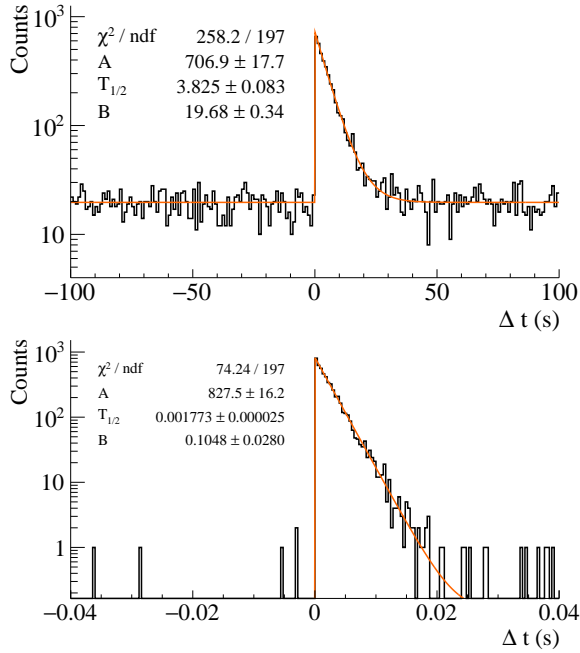


Fig. 9: Exponential fit to the Δt distribution for the $^{223}\text{Ra} \rightarrow ^{219}\text{Rn}$ (top) and $^{219}\text{Rn} \rightarrow ^{215}\text{Po}$ (bottom) α decays in the ^{235}U chain. The best-fit values are reported in the figures.

the I distribution of each identified α peak with a Gaussian function, whose position is related to the Q -value of the decay, while the FWHM of the peak is a measure of the energy resolution. We include all the α from both triplet decays except that of ^{223}Ra , since in this case γ rays are also emitted with a probability $>90\%$, introducing additional features to the I distribution. Figure 10 shows the resulting polynomial fit to the available α calibration points, including also the one from the ^{152}Gd decay. The fit gives us the α energy scale E_α , and allows us to extract the resolution curve as a function of energy for α events (Fig. 11).

The integral of the exponential fits on the Δt distributions corresponds to the number of identified decays. Taking into account the selection efficiencies of the α peaks, the duration of the data collection, and the mass of the crystal, we obtain a (2.34 ± 0.02) mBq/kg contamination value for the $^{224}\text{Ra} \rightarrow ^{220}\text{Rn} \rightarrow ^{216}\text{Po} \rightarrow ^{212}\text{Pb}$ triplet, and (1.51 ± 0.02) mBq/kg for the $^{223}\text{Ra} \rightarrow ^{219}\text{Rn} \rightarrow ^{215}\text{Po} \rightarrow ^{211}\text{Pb}$ one. As mentioned before, we find no candidate for the two TDC doublets of the ^{238}U chain.

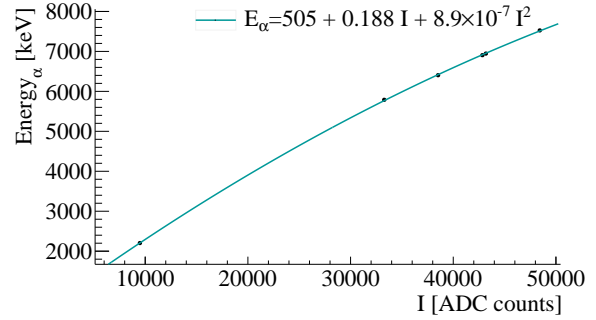


Fig. 10: Polynomial fit to the α energy, E_α , vs. pulse integral I of the α peaks identified with the delayed coincidence study plus that from ^{152}Gd .

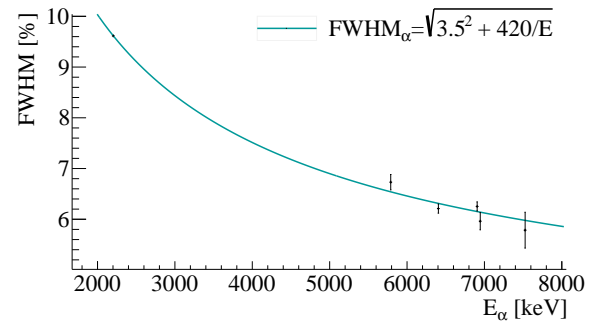


Fig. 11: FWHM as a function of energy for α events.

Considering that all isotopes of the ^{232}Th chain following ^{228}Th must be in equilibrium, we cross-check the obtained activity by searching for the $^{212}\text{Bi} \rightarrow ^{212}\text{Po} \rightarrow ^{208}\text{Po}$ β - α TDC (Tab. 2). Given the shorter half-life value of this TDC, we acquired a special run with a short acquisition window of 400 ns. To identify the events, we start from the 8.9 MeV α of the second decay and look backward in time to find the preceding β decay. When calculating the activity with this β - α coincidence, two efficiencies have to be taken into account: the first is introduced by the acquisition window of 400 ns and the digitizer dead time, which reduces the visible Δt distribution to $\sim 35\%$, and the second is the 64% branching ratio. The resulting activity is (1.9 ± 0.08) mBq/kg. This is 20% smaller than the activity measured with the α triplet, probably as a result of a poorly measured dead-time efficiency. Therefore, we consider the value measured with the α triplet as more reliable.

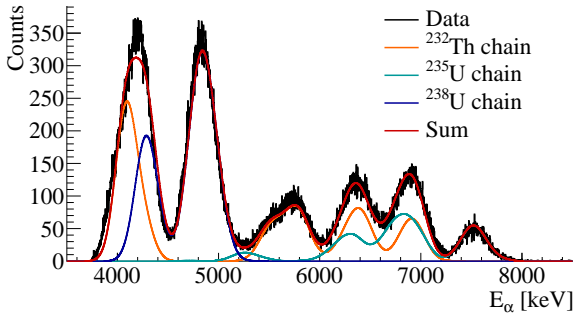


Fig. 12: Global fit (red line) to the α peaks (black points). The contribution from the individual decay chains are also reported.

Considering a different approach with respect to the TDC study, we fit the α energy spectrum with an analytical model which includes all possible α peaks of the three radioactive chains ^{232}Th , ^{238}U , and ^{235}U . The expected peak from each α decay is modeled with a Gaussian having mean centered on the Q -value of the decay and a FWHM from the fit in Fig. 11. In some decays the daughter nucleus can be produced in different excited states and de-excites by emitting one or more γ rays. In this case we construct a Gaussian for all the possible α energies weighted with their specific probability, and take into account the energy deposited by γ , constructing further Gaussian distributions using the calibration curve and energy resolution for the β/γ events. This is an approximate procedure, as the case in which the γ energy is not fully contained in the crystal is not considered. We fix the amplitudes of all peaks following ^{228}Th to 2.34 mBq/kg, and of those following ^{227}Ac to 1.51 mBq/kg. On the contrary, we keep the amplitudes of peaks in the early parts of the chains as free parameters. The fit is performed in the E_α space and the result is shown in Fig. 12. Tab. 4 summarizes the contamination values for the various part of the decay chains obtained with the TDC and the spectra fit approaches.

An activity of 8.4 mBq/kg is found for ^{232}Th α decay, a factor of 3.6 higher than the activity of the rest of the chain. The α decays in the higher part of the ^{238}U chain show an activity of 6.3 mBq/kg, while the lower part of the chain is not found in our analysis. For the ^{235}U chain, α decays of ^{235}U and ^{231}Pa are present with an activity of 0.30 mBq/kg. It is interesting to notice that this activity matches what expected based on the known isotopic ratio

of $^{235}\text{U}/^{238}\text{U}=0.7\%$ and on the lifetimes of the two isotopes. The lower part of the ^{235}U chain features a higher activity according to the measurements with the TDC analysis, pinpointing a contamination of ^{227}Ac . The total α rate which is obtained by summing up the contributions from the three radioactive chains matches the total measured α activity above the ^{152}Gd peak.

This measured background can be compared with the one obtained in similar studies of GAGG crystals [20, 21]. As for the α background, it appears that the measured contamination values are comparable for the ^{232}Th chain. The ^{238}U upper part contamination appears a factor of 20 lower in the present study. As for the ^{235}U chain, the contamination in the upper part is a factor of 10 lower in our crystal, while it is comparable in the lower part, as a result of a ^{227}Ac contamination.

5 Perspectives as neutron detector

In order to demonstrate the possibility of using GAGG crystals for neutron detection underground, we performed two AmBe calibrations, placing the source inside the borated PE shielding. In the first measurement, we placed a 5 cm thick PE moderator between the source and the detector, then we substituted the PE moderator with a 5 cm thick copper brick. Fig. 13 shows the corresponding spectra in the β/γ band: in all cases, a continuum reaching $\sim 9\text{MeV}$ is clearly visible, consisting of a combination of electrons and γ emitted from the de-excitation of ^{156}Gd and ^{158}Gd nuclei following a neutron capture on ^{155}Gd and ^{157}Gd , respectively. To our knowledge, this is the first measurement of the high-energy Gd β/γ cascades with a GAGG crystal. The spectrum also shows a peak at 4.4 MeV, corresponding to a γ emitted by the de-excitation of ^{12}C produced by the (α,n) reaction in the AmBe source, as well as its single and double-escape peaks.

To estimate the relative intensity of the Gd cascades and ^{12}C -induced events, we substituted the PE moderator with the copper brick, as previously mentioned, keeping the distance between the source and the detector unaltered. This leads to a reduction of a factor 1.6 of the continuum above

Table 4: Activities of α decays for the various parts of the ^{232}Th , ^{238}U and ^{235}U decay chains. The values marked with an asterisk are fixed according to the activity values from the TDC triplets. The total calculated α rates for each chain and for the sum of the three chains are also reported.

Radioactive chain		Total α rate [mHz/kg]	
^{232}Th		20.1 \pm 0.1	
Decay	Q-value [keV]	Method	Activity [mBq/kg]
^{232}Th	4082	α spectrum fit	8.4 \pm 0.1
^{228}Th	5520	α spectrum fit	2.34*
$^{224}\text{Ra}\rightarrow^{220}\text{Rn}\rightarrow^{216}\text{Po}$	5789, 6405, 6906	triple α coincidence	2.34 \pm 0.02
^{212}Bi	6207	α spectrum fit	2.34 \times 0.36 = 0.84*
^{212}Po	8954	α spectrum fit	2.34 \times 0.64 = 1.50*
$^{212}\text{Bi}\rightarrow^{212}\text{Po}$	2252, 8954	β - α coincidence	1.22 \pm 0.04
Radioactive chain		Total α rate [mHz/kg]	
^{238}U		18.9 \pm 0.2	
Decay	Q-value [keV]	Method	Activity [mBq/kg]
^{238}U	4270	α spectrum fit	6.3 \pm 0.1
^{234}U	4857	α spectrum fit	6.3 \pm 0.1
^{230}Th	4770	α spectrum fit	6.3 \pm 0.1
^{226}Ra	4871	α spectrum fit	Not found
$^{222}\text{Rn}\rightarrow^{218}\text{Po}$	5590, 6115	double α coincidence	Not found
$^{214}\text{Bi}\rightarrow^{214}\text{Po}$	3269, 7834	β - α coincidence	Not found
^{210}Po	5407	α spectrum fit	Not found
Radioactive chain		Total α rate [mHz/kg]	
^{235}U		8.2 \pm 0.1	
Decay	Q-value [keV]	Method	Activity [mBq/kg]
^{235}U	4678	α spectrum fit	0.30 \pm 0.05
^{231}Pa	5150	α spectrum fit	0.30 \pm 0.05
^{227}Th	6146	α spectrum fit	1.51*
$^{223}\text{Ra}\rightarrow^{219}\text{Rn}\rightarrow^{215}\text{Po}$	5979, 6946, 7526	triple α coincidence	1.51 \pm 0.02
^{211}Bi	6750	α spectrum fit	1.51*
Total α rate ($^{232}\text{Th}+^{238}\text{U}+^{235}\text{U}$)		(47.2 \pm 0.2) mHz/kg	

5 MeV, caused by the absence of the PE moderator, and of a factor 2.4 in the region containing the 4.4 MeV peak and its escape peaks, caused by the copper presence. On the contrary, the two spectra match very well below \sim 2.7 MeV, showing that the neutron contribution is negligible in comparison to the intrinsic background in that energy range. At present, we do not yet have a thorough evaluation of the overall detector efficiency. This is only achievable via Monte Carlo simulations, which are currently under development.

Finally, we acquired one month of data with the unshielded detector to measure the thermal neutron flux. The corresponding spectrum is shown in teal in Fig. 13, showing an overall higher count rate than in the background spectrum, which has different causes, depending on the energy region. The absence of the borated PE shielding causes a higher rate in the environmental γ which dominates the spectrum up to the 2615 keV line from ^{208}Tl , and also causes an increase in event rate up to \sim 3.2 MeV, due to the higher probability for the 2615 keV and the 583 keV lines, which are in true coincidence

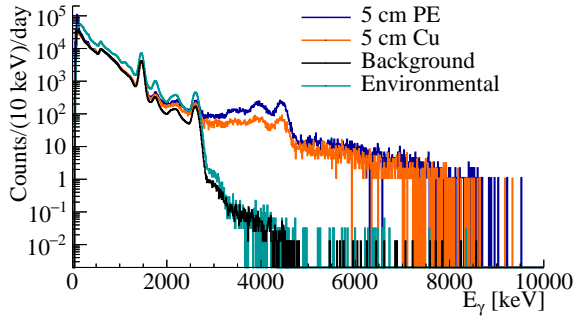


Fig. 13: β/γ spectra obtained with the AmBe calibration and environmental neutron measurements. The AmBe spectra in blue and red are obtained from the two measurements with a PE moderator and a copper brick placed between the source and the detector, respectively. The background spectrum is measured with the detector shielded by the borated PE, while the environmental refers to the thermal neutron measurement with no shield.

in 85% of the cases, to be both fully absorbed by the detector. On the other hand, the higher rate above 3.2 MeV can only be attributed to neutron-induced events.

Tab. 5 reports the count rates obtained from the measurements with the shielded and unshielded detector over different energy ranges. The region above 5 MeV is only populated by neutron-induced events, but suffers from a limited containment efficiency for the Gd de-excitation γ 's. Expanding the counting region to lower energies allows to include a higher fraction of neutron events, at the cost of accepting also a higher background. Converting the net neutron event rates to flux values, we obtain estimates in the $[0.5 - 1] \cdot 10^{-6}$ neutrons/cm²/s, in agreement with previous measurements of thermal neutrons performed at LNGS [22–24]. In the future, we plan to optimize the counting region by means of dedicated simulations.

6 Conclusions and outlook

In this article, we have demonstrated the possibility to effectively employ large volume GAGG crystals for the measurement of neutrons, thanks to the detection of the electron and γ cascades emitted by the ¹⁵⁶Gd and ¹⁵⁸Gd de-excitation. An advanced frequency-based PSD algorithm has

Table 5: Count rates obtained from the background measurement and the environmental neutron measurement in different energy ranges. The last column reports the net count-rate difference between the environmental and background rates, attributed to neutron-induced events.

ΔE [MeV]	Background [counts/day]	Environmental [counts/day]	Net neutrons [counts/day]
[3.5, 10]	5.1 ± 0.3	6.3 ± 0.4	1.1 ± 0.5
[4.0, 10]	1.7 ± 0.2	2.9 ± 0.3	1.2 ± 0.3
[4.5, 10]	0.45 ± 0.08	1.0 ± 0.2	0.6 ± 0.2
[5.0, 10]	0.28 ± 0.06	0.7 ± 0.2	0.4 ± 0.2

allowed us to fully separate the α from the β/γ events. Applying a delayed-coincidence analysis to the α spectrum, we have measured with $\leq 20\%$ precision the contamination values of all parts of the ²³²Th, ²³⁸U, and ²³⁵U decay chains. Dedicated AmBe calibrations have confirmed the GAGG potential for neutron detection, and the preliminary measurement of environmental neutrons in the Hall A of LNGS is in good agreement with previous results obtained with different detectors in the same location. The main background is represented by the intrinsic ²³²Th contamination, which induces a continuum in the β/γ band reaching 5 MeV. Reducing the ²³²Th contamination below the 0.1 mBq/kg is crucial for enhancing the detector sensitivity to neutrons.

In the near future, we aim to develop a full simulation of the neutron interaction in the detector, and of the propagation of the electron and γ rays emitted by the Gd de-excitation following a neutron capture. Such simulations will allow us to evaluate the total detection efficiency, and to design a larger setup consisting of several detectors coupled to Bonner spheres for measuring the neutron spectrum at LNGS and in other underground laboratories.

As for using the GAGG detectors above ground to measure neutrons, the fundamental limitation is the impossibility to distinguish the neutron-induced β/γ events from the overwhelming muon background. In the long term, we intend to bypass this limitation by inserting a GAGG crystal into a plastic-scintillator case with a thickness of several centimeters, which would act both as a neutron moderator and a muon veto. Such a design could allow to effectively operate GAGG

crystals for above-ground neutron detection, and provide a valid and affordable alternative to ^3He counters.

Acknowledgements. This work was supported by the EU Horizon2020 research and innovation program under the Marie Skłodowska-Curie Grant Agreement No. 754496, and by the European Union, Next Generation EU, Mission 4 Component 1, CUP 2022WWRZZP_001.

References

- [1] Kamada, K., *et al.*: Crystal Growth and Scintillation Properties of Ce Doped $\text{Gd}_3(\text{GaAl})_5\text{O}_{12}$ Single Crystals. *IEEE Trans. on Nucl. Sci.* **59**(5), 2112–2115 (2012) <https://doi.org/10.1109/TNS.2012.2197024>
- [2] Kobayashi, M., *et al.*: Significantly different pulse shapes for gamma- and alpha-rays in $\text{Gd}_3\text{Al}_2\text{Ga}_3\text{O}_{12}:\text{Ce}^{3+}$ scintillating crystals. *Nucl. Instrum. Meth. A* **694**, 91–94 (2012) <https://doi.org/10.1016/j.nima.2012.07.055>
- [3] Iwanowska, J., *et al.*: Performance of cerium-doped $\text{Gd}_3\text{Al}_2\text{Ga}_3\text{O}_{12}$ (GAGG:Ce) scintillator in gamma-ray spectrometry. *Nucl. Instrum. Meth. A* **712**, 34–40 (2013) <https://doi.org/10.1016/j.nima.2013.01.064>
- [4] Tamagawa, Y., *et al.*: Alpha–gamma pulse-shape discrimination in $\text{Gd}_3\text{Al}_2\text{Ga}_3\text{O}_{12}$ (GAGG):Ce $^{3+}$ crystal scintillator using shape indicator. *Nucl. Instrum. Meth. A* **795**, 192–195 (2015) <https://doi.org/10.1016/j.nima.2015.05.052>
- [5] Taggart, M.P., Nakhostin, M., Sellin, P.J.: Investigation into the potential of GAGG:Ce as a neutron detector. *Nucl. Instrum. Meth. A* **931**, 121–126 (2019) <https://doi.org/10.1016/j.nima.2019.04.009>
- [6] Tyagi, M., *et al.*: Development of Neutron Detector Based on $\text{Gd}_3\text{Ga}_3\text{Al}_2\text{O}_{12}:\text{Ce}$ Single Crystals. *IEEE Trans. on Nucl. Sci.* **66**(4), 724–728 (2019) <https://doi.org/10.1109/TNS.2019.2900440>
- [7] Fedorov, A., *et al.*: Sensitivity of GAGG based scintillation neutron detector with SiPM readout. *Nucl. Eng. and Tech.* **52**(10), 2306–2312 (2020) <https://doi.org/10.1016/j.net.2020.03.012>
- [8] Fedorov, A., *et al.*: Pulse shape discrimination at the registration of 14.6 MeV neutrons with $\text{Gd}_3\text{Ga}_3\text{Al}_2\text{O}_{12}:\text{Ce}/\text{SiPM}(\text{PMT})$ detectors. *Nucl. Instrum. Meth. A* **1062**, 169155 (2024) <https://doi.org/10.1016/j.nima.2024.169155>
- [9] Wang, Z., *et al.*: Performance study of GAGG:Ce scintillator for gamma and neutron detection. *JINST* **15**(06), 06031 (2020) <https://doi.org/10.1088/1748-0221/15/06/C06031>
- [10] Litaize, O., *et al.*: Fission modelling with FIFRELIN. *Eur. Phys. J. A* **51**(12), 177 (2015) <https://doi.org/10.1140/epja/i2015-15177-9>
- [11] Almazán Molina, H., *et al.*: Improved STEREO simulation with a new gamma ray spectrum of excited gadolinium isotopes using FIFRELIN. *Eur. Phys. J. A* **55**(10), 183 (2019) <https://doi.org/10.1140/epja/i2019-12886-y>
- [12] Mendoza, E., *et al.*: NuDEX: A new nuclear γ -ray cascades generator. *EPJ WoC* **239**, 17006 (2020) <https://doi.org/10.1051/epjconf/202023917006>
- [13] Article in preparation
- [14] Lee, H.S., *et al.*: Pulse-shape discrimination between electron and nuclear recoils in a NaI(Tl) crystal. *JHEP* **08**, 093 (2015) [https://doi.org/10.1007/JHEP08\(2015\)093](https://doi.org/10.1007/JHEP08(2015)093) [arXiv:1503.05253](https://arxiv.org/abs/1503.05253)
- [15] Tamagawa, Y., *et al.*: Alpha–gamma pulse-shape discrimination in $\text{Gd}_3\text{Al}_2\text{Ga}_3\text{O}_{12}$ (GAGG):Ce $^{3+}$ crystal scintillator using shape indicator. *Nucl. Instrum. Meth. A* **795**, 192–195 (2015) <https://doi.org/10.1016/j.nima.2015.05.052>
- [16] Nisi, S.: Private communication
- [17] Baccolo, G., *et al.*: Improving radioactive

- contaminant identification through the analysis of delayed coincidences with an α -spectrometer. *Eur. Phys. J. C* **81**(11), 971 (2021) <https://doi.org/10.1140/epjc/s10052-021-09759-5>
- [18] Azzolini, O., *et al.*: Background identification in cryogenic calorimeters through $\alpha - \alpha$ delayed coincidences. *Eur. Phys. J. C* **81**(8), 722 (2021) <https://doi.org/10.1140/epjc/s10052-021-09476-z>
- [19] IAEA Interactive Chart of Nuclides. <https://www-nds.iaea.org/relnsd/vcharthtml/VChartHTML.html> Accessed April 2025
- [20] Omori, T., *et al.*: First Study of the PIKACHU Project: Development and Evaluation of High-Purity $\text{Gd}_3\text{Ga}_3\text{Al}_2\text{O}_{12}:\text{Ce}$ Crystals for ^{160}Gd Double Beta Decay Search. *PTEP* **2024**(3), 033–01 (2024) <https://doi.org/10.1093/ptep/ptae026>
- [21] Omori, T., *et al.*: Simulation Tool Development and Sensitivity Analysis of ^{160}Gd Double Beta Decay Search by the PIKACHU Project (2024) [arXiv:2412.04712](https://arxiv.org/abs/2412.04712) [hep-ex]
- [22] Best, A., *et al.*: Low energy neutron background in deep underground laboratories. *Nucl. Instrum. Meth. A* **812**, 1–6 (2016) <https://doi.org/10.1016/j.nima.2015.12.034> [arXiv:1509.00770](https://arxiv.org/abs/1509.00770)
- [23] Belli, P., *et al.*: Deep Underground Neutron Flux Measurement With Large BF_3 Counters. *Nuovo Cim. A* **101**, 959–966 (1989) <https://doi.org/10.1007/BF02800162>
- [24] Wulandari, H., *et al.*: Neutron flux underground revisited. *Astropart. Phys.* **22**, 313–322 (2004) <https://doi.org/10.1016/j.astropartphys.2004.07.005> [arXiv:hep-ex/0312050](https://arxiv.org/abs/hep-ex/0312050)